Results in Engineering 16 (2022) 100603

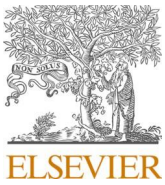

Contents lists available at ScienceDirect

Results in Engineering

journal homepage: www.sciencedirect.com/journal/results-in-engineering

Influence of loading sequence on wind induced fatigue assessment of bolts in TV-tower connection block

S. Chowdhury [a,*], V. Zabel [b]

[a] Bauhaus University Weimar, Chair of Steel and Hybrid Structures, Marienstrasse 13D, 99423, Weimar, Germany
[b] Bauhaus University Weimar, Institute of Structural Mechanics, Marienstrasse 15, 99423, Weimar, Germany

ARTICLE INFO

Keywords:
Fatigue life
TV Tower
Wind load
Rainflow counting algorithm
Loading sequence
Structural health monitoring
Damage accumulation

ABSTRACT

Bolted connections are widely employed in structures like transmission poles, wind turbines, and television (TV) towers. The behaviour of bolted connections is often complex and plays a significant role in the overall dynamic characteristics of the structure. The goal of this work is to conduct a fatigue lifecycle assessment of such a bolted connection block of a 193 m tall TV tower, for which 205 days of real measurement data have been obtained from the installed monitoring devices. Based on the recorded data, the best-fit stochastic wind distribution for 50 years, the decisive wind action, and the locations to carry out the fatigue analysis have been decided. A 3D beam model of the entire tower is developed to extract the nodal forces corresponding to the connection block location under various mean wind speeds, which is later coupled with a detailed complex finite element model of the connection block, with over three million degrees of freedom, for acquiring stress histories on some pre-selected bolts. The random stress histories are analysed using the rainflow counting algorithm (RCA) and the damage is estimated using Palmgren-Miner's damage accumulation law. A modification is proposed to integrate the loading sequence effect into the RCA, which otherwise is ignored, and the differences between the two RCAs are investigated in terms of the accumulated damage.

1. Introduction

Wind-induced fatigue is a prominent failure mode in television (TV) towers since they are slender and tall structures that are constantly subjected to dynamic and random wind loading during their service life [1,2]. The fatigue analyses of such structures under wind loads can be performed in the time domain and in the frequency domain, where the first one deals with the conventional cycle counting procedures and the second one is with a probabilistic approach. The leading works in the frequency domain are conducted by Davenport [3,4] by incorporating fundamental random dynamics ideas [5]. In this method, the overall damage is determined by accounting for the probability that the fluctuating stress processes connected to various mean wind velocity values will occur [6,7]. Contrary to this, time-domain studies can be performed using pressure measurements retrieved from the experiments, such as during wind tunnel testing [8] or by stochastically simulating the turbulence histories using the Monte Carlo algorithm [9–11]. However, the fatigue assessment in the time domain follows a classical deterministic approach—the variable stress signals generated under different mean wind speeds are converted into equivalent multiple constant amplitude stress signals followed by applying some cycle counting techniques such as the rainflow counting method. In certain instances, these approaches allow for the portrayal of the cycle-histogram to offer helpful indicators to comprehend the physical phenomena [12,13], as opposed to just analyzing the mean cumulative damage or the fatigue life. Recent applications of such approaches to wind turbine blade damage are reviewed in Refs. [14,15]. Within the scope of this study, only the deterministic time domain method with rainflow counting is evaluated.

In 1968, Tatsuo Endo and M. Matsuishi proposed the rainflow counting algorithm (RCA) [16], which can break down loading histories to extract the amplitudes, mean values and frequencies of stress histories for a certain period and produce the information as a so-called rainflow matrix format [17,18]. This algorithm is the most extensively used and adapted in the stress-life strategy (SN theory) of fatigue evaluation, specifically in the damage accumulation hypothesis provided by Palmgren–Miner [19,20]. The algorithm proposed in Ref. [16], on the other hand, is designed in such a manner that the loading sequence effects are completely disregarded, resulting in the omission of particular stress ranges. In terms of fatigue life evaluation, neglecting the loading sequence might be critical as the stress difference plays a significant role

* Corresponding author.
E-mail addresses: sharmistha.chowdhury@uni-weimar.de (S. Chowdhury), volkmar.zabel@uni-weimar.de (V. Zabel).

https://doi.org/10.1016/j.rineng.2022.100603
Received 21 July 2022; Received in revised form 18 August 2022; Accepted 20 August 2022
Available online 28 August 2022

in damage calculation. In this study, a modification is therefore proposed to the RCA to account for the loading sequence, and subsequently, the changes in damage calculation are interpreted.

Efficient finite element models are a prerequisite to retrieving the reliable stress histories of the structure. Due to the intricate nature of the structure and the loading pattern, numerical simulations of connection blocks under wind loading are generally computationally expensive and time-consuming. The most frequent practise for resolving this issue is to develop a simplified metamodel for approximating the numerical model. Conventional metamodels, also named surrogate models, are approximated entities to capture the relation between load and structural response as a result of the actual behaviour of the structure and can be adapted to predict the stress histories from a limited number of numerical analyses [21,22]. However, the decisive wind action must be determined prior to numerical analysis. TV towers usually feature a distinct profile consisting of different structural shapes, e.g., circular observation decks and support systems with vertical or flared legs and bolts, a configuration essential to sustain the extreme height, though susceptible to dynamic wind forces. The aerodynamics of these towers are greatly influenced by structural changes, particularly on the continuity in the profile geometry, which governs the critical wind action [23,24]. One of the significant wind actions for tall structures is *vortex induced vibration* (VIV), which are motions induced on bodies interacting with an external fluid flow, produced by periodical irregularities on this flow [25,26]. This phenomenon occurs particularly on structures with circular or nearly circular cross-sections. Another important wind action is *buffeting* of turbulence in the along-wind direction and wake excitation in the across-wind direction [1,27,28].

Engineering structures like towers, which are susceptible to environmental loading with a complex nature, need frequent monitoring because of their long life expectancy from the authorities, and thus the life cycle assessment often comes as the priority to be addressed. The investigated TV tower contains a connecting block that is assisted by many M80.6 sized bolts, and fatigue investigation of some bolts is prioritized in the interest of the authorities. The TV tower has been instrumented with anemometers, accelerometers, and temperature sensors for over a year. Lifetime prediction of such unique structures is often challenging, not only because of the complexity regarding loadings, numerical modelling, or data assessment but also due to the lack of suitable practical examples. Therefore, the methodology used in this research is as follows: In section 2, the numerical modelling of the global tower, the connection block and the coupling between these two models are presented. Section 3 involves the stochastic wind analysis of the structure based on the installed monitoring scheme. During the monitoring period, the characteristic features of the wind force, such as mean wind speed and corresponding frequency, are recorded, and the decisive wind action has been determined based on the acceleration and corresponding wind speeds. The measured data afterwards was used to forecast the best fit for 50-year wind distribution. In section 4, the numerical stresses under various wind speeds are extracted using the model developed in section 2. To overcome the inefficiency of the simulation, a meta-model approach to stress history analysis has been developed. Section 5 discusses the stress-based fatigue analysis, which in further steps investigates the influence of two considered RCAs in the damage calculation.

2. Numerical modelling

The investigated TV tower with 192.85 m height is located in Germany and was constructed during the early 1970s. The tower is comprised of concrete, steel and fibreglass, and features two major connection blocks – the first one is at the transition between the concrete and the steel section, and the second one is between the steel and the fibreglass section. A simplified geometrical overview of the tower is shown in Fig. 1(a), and an overview of the material parameters is given in Table 1, which has been collected from the normative documents provided by the owner. The details of these connection blocks are very sophisticated and require precise modelling to predict any possible damage as they integrate various sizes and numbers of connection details.

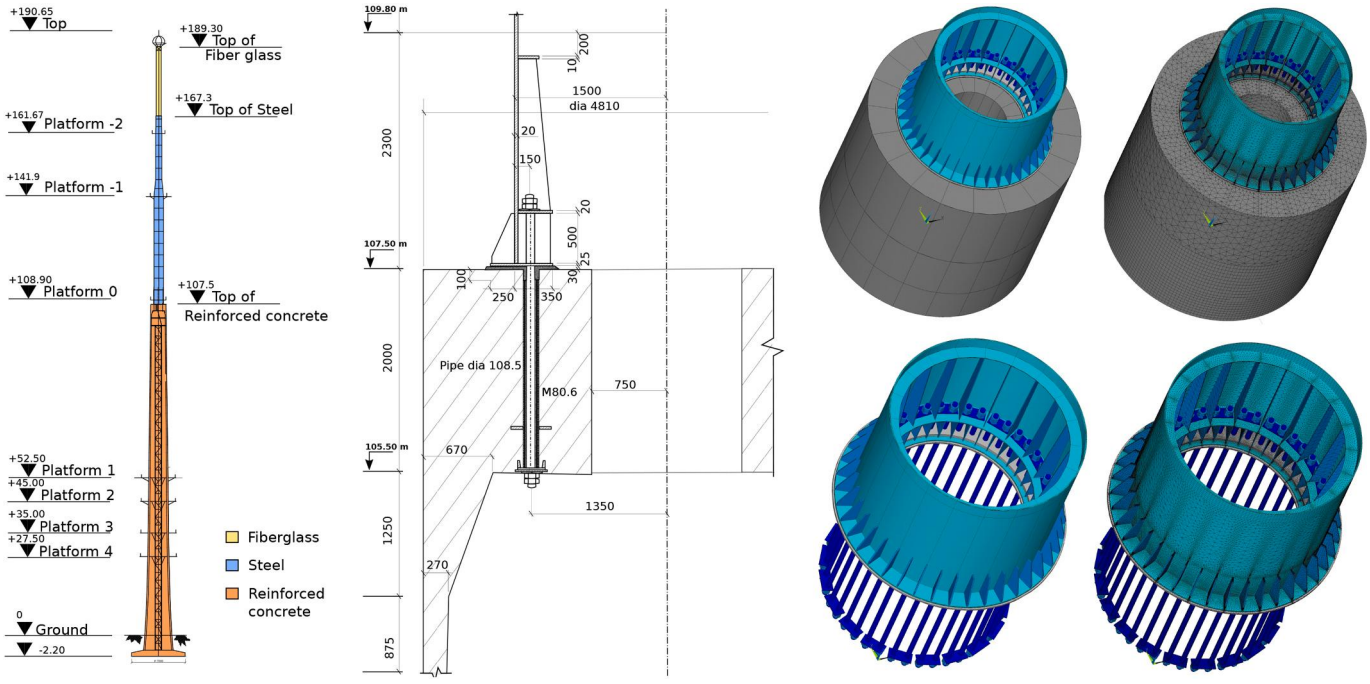

Fig. 1. Numerical detailing of the connection block between steel and concrete section. (a) Geometrical overview of the TV tower. (b) Longitudinal cross-section of the connection block (all dimensions are in mm unless mentined). (c) A detailed finite element model of the connection block between steel and concrete section.

Table 1
Details of material parameters obtained from the normative document provided by the authority and used in the finite element model.

	Density	Young's modulus	Poisson's Ratio	Height	Outer Dia.	Inner Dia.
	ρ [kg/m3]	E [MPa]	ν	h [m]	d_o [m]	d_i [m]
Concrete	2.50E+03	3.00E+10	0.20	0–107.5		
Steel	7.85E+03	2.10E+11	0.30	107.5–141.9	1.50	1.45
	7.85E+03	2.10E+11	0.30	141.9–146.9	1.25	1.2
	7.85E+03	2.10E+11	0.30	146.9–159.9	1	0.95
	7.85E+03	2.10E+11	0.30	159.9–167.3	0.9	0.85
Fibreglass	2.60E+03	7.30E+10	0.22	167.3–189.3	0.675	0.665

2.1. Global modelling

A 3D simplified computational beam model of the whole tower system has been developed to evaluate the impact of along-wind direction forces that can determine the load impacts in each section of the structure. The stochastic wind loading at different wind speeds has also been simulated in the finite element package. Details about the computational wind load modelling are discussed in section 3.

2.2. Modelling of bolted connection block

The first connection block located at around 108 m consists of two materials: reinforced concrete and steel. One basic comprehensive model has been developed using documents provided by the tower project personnel, as well as referring to project supervision records. A simple cross-section of the connection block prototype is shown in Fig. 1 (b). The total height of the connection block, modelled for numerical analyses, is 6495 mm where 4195 mm is of reinforced concrete, and the rest belongs to the steel part. The lower 4195 mm concrete section can be subdivided into three different regions:

1. The most bottom hollow section with 875 mm height, and 270 mm thickness,
2. A tapered hollow section with a height of 1250 mm and a section thickness varying from 270 mm at the bottom to 670 mm at the top, and
3. The top hollow section where the section thickness is 1655 mm and the height is 2000 mm.

The steel part, which starts immediately above the concrete section, is connected via 40 pieces of type M80.6 bolts. A 30 mm thick plain concrete layer is integrated into the connecting block slightly above the reinforced concrete section, allowing a 25 mm thick solid steel plate to be added above it. In addition, various types of steel connection plates are employed to assist bonding between the reinforced concrete and steel section, which is taken into account in the numerical modelling of the connection block, as shown in Fig. 1(c). As per the authorities, the tower bolts are only prestressed by tightening torque. Details on the tightening torque and requirements for different bolts can be found in Ref. [29]. The adequate amount of torque to tighten the M80.6 bolts was calculated based on the following relations:

$$S_T = \frac{S_E}{\sqrt{\left[1+3\times\left\{\left(\frac{4\times d_2}{d_2+d_3}\right)\times\left(\left[\frac{P_t}{\pi\times d_2}\right]+[1.155\times\kappa_T]\right)\right\}\right]^2}} \tag{1}$$

$$F_p = S_T \times A_s \quad \text{where} \quad A_s = \frac{(d_2+d_3)^2}{16} \tag{2}$$

$$T_{torque} = F_p \times \left[\left(0.159+P_t\right)+(0.577\times d_2\times\mu_T)+\left(d_f\times\frac{\mu_H}{2}\right)\right] \tag{3}$$

Here, S_T = tensile stress, F_p = preload and T_{torque} = tightening torque; S_E = equivalent stress, d_2 = pitch diameter of the thread, d_3 = minor diameter of the thread, P_t = pitch length of the thread, κ_T = thread friction coefficient, d_f = effective friction diameter of the bolt head or nut.

The numerical model of the connection block is created in the finite element package Ansys with higher-order tetrahedral 3D volume elements. These elements are defined by 10 nodes with three degrees of freedom at each node and quadratic displacement behaviour [30]. Additionally, multi-point constraints (MPC) elements are utilized to supplement the constraints introduced from the global model to the local model, specifically at the top and bottom of the connection block to transfer the internal loading forces from the global model. Details on the MPC elements can be found in Ref. [31]. Fig. 1(c) shows the comprehensive 3D volume element-based model of the block, which consists of around 3 million degrees of freedom.

3. Stochastic wind load analysis

3.1. Determination of decisive wind load action

The TV tower was under monitoring containing accelerometers, anemometers and temperature sensors to measure the acceleration, the wind speed and direction, and temperature, respectively. Two anemometers and two accelerometers are installed – a) at 108 m where the reinforced concrete - steel connection block is located and b) at 188 m.

The investigated tower has a tapered circular section, which renders it susceptibility to *vortex induced vibration* (VIV). The VIV action can be observed on a structure for a limited range of wind speed or under critical wind speed, while the *buffeting* action occurs for any range of turbulent wind speed, see Fig. 2(a). The rms acceleration(root mean squared) and the mean wind speed, averaged over 10 min period, are extracted from the monitoring system for 265 days and are plotted in Fig. 2(b). Based on this observation, it is clear that at any given wind speed, no major peak is visible to evaluate VIV action. Furthermore, the externally installed antennas on the tower considered here are attached to the steel section (from 109 m to 190 m), making it more resistant to VIV-induced activity. The VIV action is supposed to be additionally understated by the tuned mass damper mounted at the fibreglass section. Given these characteristics, it is therefore conclusive that the decisive wind load action is *buffeting*, which is further incorporated in the numerical stress analysis.

3.2. Buffeting analysis

Under the influence of wind flow, structures can experience two types of aerodynamic responses: static and dynamic. The aerodynamic forces on the structure determine these responses – with the drag force (along-wind) acting in the mean wind direction and the lift force (cross-wind or transverse) acting in the perpendicular direction. Wind fluctuations are primarily responsible for the aerodynamic response of slender structures, and these responses are more significant for structures with lower fundamental frequencies.

The wind rose diagrams of the measured data from both anemometers for 265 days are shown in Fig. 3. At +108 m height, the dominant wind speed of the tower is from the west to the south-west, while the

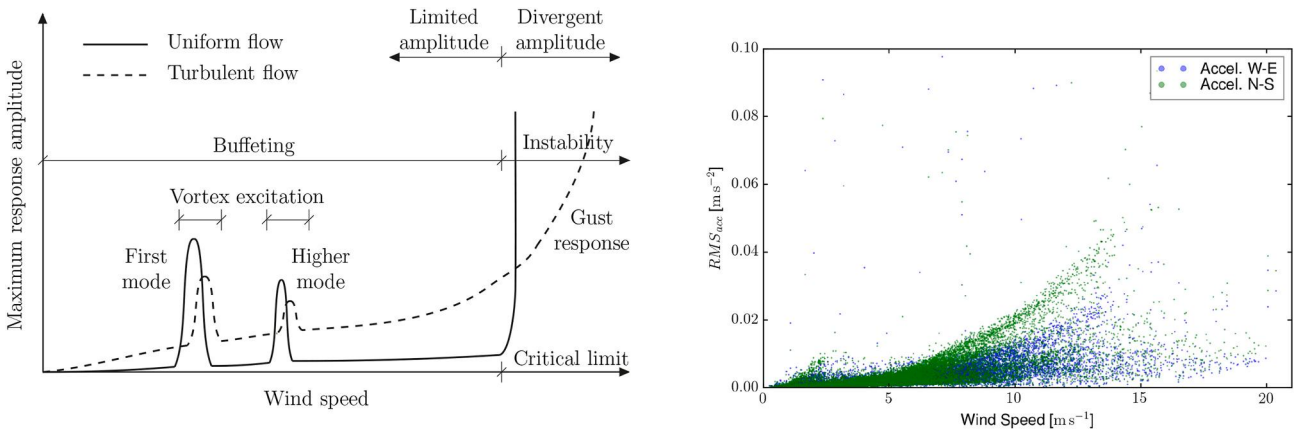

Fig. 2. Selection of the decisive wind action based on the recorded 205 days of measurement data. (a) Schematic of structural response against wind speed [32]. (b) Root mean square acceleration obtained from the installed accelerometers (at 188 m) depending on the 10-minutes mean wind speed [33].

secondary strong wind is generated from the south-east. The substantial secondary strong wind in the direction of the tower is only recognized up to the connection block, see Fig. 3(a); however, the wind rose diagram from the top anemometer, installed at +188 m height, explicitly shows that the fibreglass section does not maintain such a strong wind from South-East, see Fig. 3(b).

The buffeting analyses using synthetic stochastic wind were performed on the global model for deriving the resultant internal forces of the structure. The forces generated by the chosen nodes, as later mentioned in Fig. 6 were subsequently applied to the connection block's local model. As a result, the stochastic wind time histories were generated using mean wind speed and turbulent intensities from the data presented in Table 3. The turbulent intensities are estimated using the preliminary analysis of the measured data by the anemometers installed on the tower, as described in Refs. [34,35]. The wind loads were evaluated using the terrain-based design wind speed specified in design standards, which later helped to determine the computational wind loads.

Since the primary goal of the study is conducting a life cycle assessment, numerous wind loading characteristics had to be considered, which essentially requires simulating numerous wind loading conditions, ranging from very low to design wind speeds. The mean wind profile was defined using the power law, and the von Karman spectrum was utilized to describe wind turbulence [36]. Wind time histories were constructed in longitudinal, and lateral directions for each node of the global beam element model of the tower. Being a very tall construction, the vertical component of wind is the least of significance, and so is omitted in the current analysis. The static wind coefficient of the segment was used to convert the wind speed time histories to forces. Besides, the cross-section of the tower was assumed to be circular, and the coefficient of drag was set to 1.2. The 10-year maximum wind speed based on site statistics is equal to 50 m/s at 10 m height, according to the Eurocode Design Standard [37]. As a result, the investigated 10-min mean wind speed for computing forces from the tower's beam model ranged from 0 to 50 m/s.

Based on wind speed, structural cross-section, and terrain condition

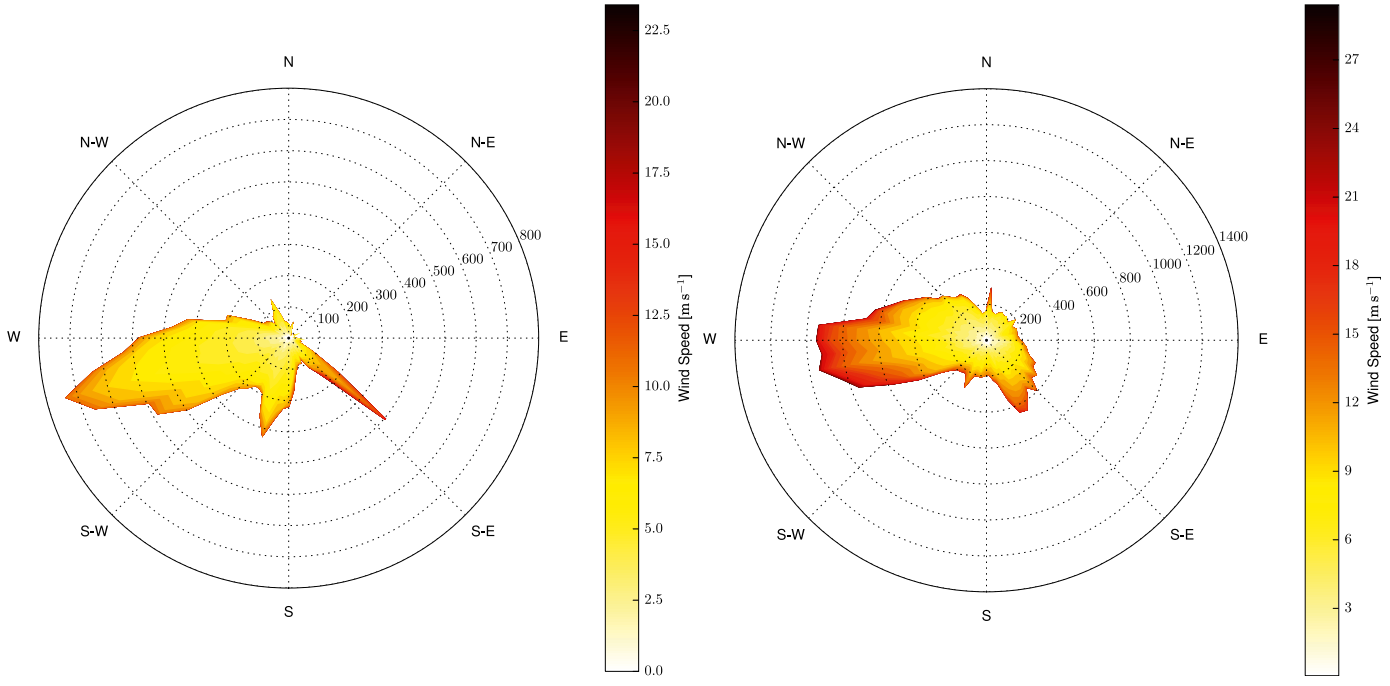

(a) Annemometer at +108 m (b) Annemometer at +188 m

Fig. 3. Wind rose representation of the data obtained from the installed two anemometers on the tower [33].

Table 2
Mean and standard deviation of the nodal moments at 109.8 m of the tower under different wind speeds.

Wind Speed	Nodal moment, M_x [KN.m]				Nodal moment, M_y [KN.m]			
(m/s)	Min	Max	Mean	Std Deviation	Min	Max	Mean	Std Deviation
			μ_{M_x}	σ_{M_x}			μ_{M_y}	σ_{M_y}
0	0	0	0	0	0	0	0	0
5	−292	−5	−154	32	−34	28	−1	−1
10	−1193	−22	−622	131	−193	183	−5	50
15	−2407	−40	−1407	313	−539	435	0	146
20	−6216	−23	−2451	788	−1216	1166	6	343
25	−8441	−155	−3949	1167	−1756	2074	−12	605
30	−11602	480	−5784	1893	−2783	3176	4	849
35	−17219	2266	−8090	2861	−3773	3768	−7	1254
40	−21428	1126	−10319	3452	−6845	8400	13	2298
45	−29402	321	−13207	4432	−9346	9478	−24	2946
50	−38117	1319	−16738	5809	−12389	10,674	−49	3873

of the tower, the following relationships were employed to derive computational time-varying wind forces.

$$U_y(t) = U_{mean} + U_{mean} \times u_y(t) \quad , \quad U_x(t) = U_{mean} \times u_x(t) \tag{4}$$

$$F_D(t) = \frac{1}{2}\rho_a U_y^2(t) D_s C_D \quad , \quad F_L(t) = \frac{1}{2}\rho_a U_x^2(t) D_s C_L \tag{5}$$

where $U_y(t)$ = wind speed in y direction, $U_x(t)$ = wind speed in x direction, $F_D(t)$ = drag force, and $F_L(t)$ = lift force; U_{mean} = mean wind speed at 10 m height, u_x = fluctuating component of wind speed along the x-axis, u_y = fluctuating component of wind speed along the y-axis, ρ_a = air density, C_D = static wind coefficient for drag, C_L = static wind coefficient for lift, F_L = lift force, F_D = drag force, and D_s = section diameter. The time history studies were carried out utilizing the Newmark-beta time-integration methodology with averaged acceleration and the ensuing response. Following the initiation of the wind forces, the time histories of the resultant internal force from the global model were transformed into the localized detail model of the connection block.

Table 2 lists the resultant nodal moments M_x = internal moment about x-axis, and M_y = internal moment and M_y, for ten distinct wind speeds ranging from 5 to 50 m/s with a 5 m/s interval. For the associated wind speeds, the minimum, maximum, mean, and standard deviation of the nodal moments are also determined. In Fig. 4 and Fig. 5, the relationship between the wind speeds and corresponding mean nodal moments, and sample nodal forces over 100 s are plotted, respectively. The absolute mean and standard deviation of nodal bending moments M_x increase as wind speed increases, following a 2nd order polynomial relationship, see Fig. 4(a) and (b). The nodal bending moment M_y, on the other hand, shows zero mean irrespective of wind speed. Similar to X-direction nodal moments, the standard deviation of nodal moments increases with increasing wind speed, Fig. 4(c) and (d). These correlations between nodal forces and wind speeds aid in reducing many simulations of the global model under various wind speeds, decreasing the number of couplings between the global model and the connection block.

3.3. Coupling between global model and connection block

A numerical coupling is introduced by integrating the resultant nodal inner moment of the global model into the local model of the connection block, see in Fig. 6. The schematic is shown for a specific wind speed, however it can be used for any other wind speed. The top and bottom nodes in the local model for introducing the forces were recognized as corresponding nodes from the global model. The resultant nodal moments were introduced to the top node of the connection block model at 109.8 m. An equivalent spring constant was introduced to the bottom node at 103.305 m which can be determined by applying unit loads at the top of the global model. The drag and lift forces were estimated using the Eurocode-1 [37] for a given mean wind speed U_{mean}.

3.4. Prediction of lifetime wind loading

The identification of the optimal stochastic distribution type is necessary in order to estimate the wind speed range over a certain lifetime span. As the data from the measuring technique only covers a limited time span, it has been fitted to multiple distribution types to determine the optimal one under specific geographical and environmental variables from Eurocode [37]. Seven distinct distribution patterns have been fitted to the data from the top anemometer in Fig. 7. Based on the computed AIC (Akaike Information Criteria) and BIC (Bayesian Information Criteria) values, a Weibull distribution is found to be the most suited distribution in this circumstance. As a consequence, the frequency of individual wind speeds may be calculated, which will be used in fatigue estimates later.

4. Numerical stress analysis

Based on the observations from the wind rose, as shown in Fig. 3 and discussed in section 3.2, a few bolts and sections in the steel shaft for installing sensors have been suggested, shown in Fig. 8. The steel shaft, however, showed no visible cracks or other damage throughout the inspection. Regarding the bolts, the only visible area of them is above 107.5 m of the tower, with an exposed height of approximately 500 mm. This study will aspect at the fatigue damage of six bolts - bolts 12, 14, and 15 which are placed in the along-wind direction, and bolts 6, 7, and 10 placed in the cross-wind direction, as indicated in Fig. 8. From a single section of one bolt, four nodal points are considered to extract the stress histories, as listed in Table 4. Fig. 8 and Table 4, respectively, show the local coordinates for the connection block and the bolt nodes.

The Von Mises stress distribution in the connection block under

Table 3
Wind characteristics at 10 m height above ground used for generating wind time histories for buffeting analysis.

Mean wind speed	Longitudinal turbulent intensity (TI)	Lateral TI	Vertical TI	Longitudinal length scale (LS)	Vertical LS	Lateral LS
U_{mean}	$I_{lon}[-]$	$I_{lat}[-]$	$I_{ver}[-]$	$L_{lon}[-]$	$L_{lat}[-]$	$L_{ver}[-]$
(m/s)				(m)	(m)	(m)
5–50	0.15	0.11	0.08	140	40	15

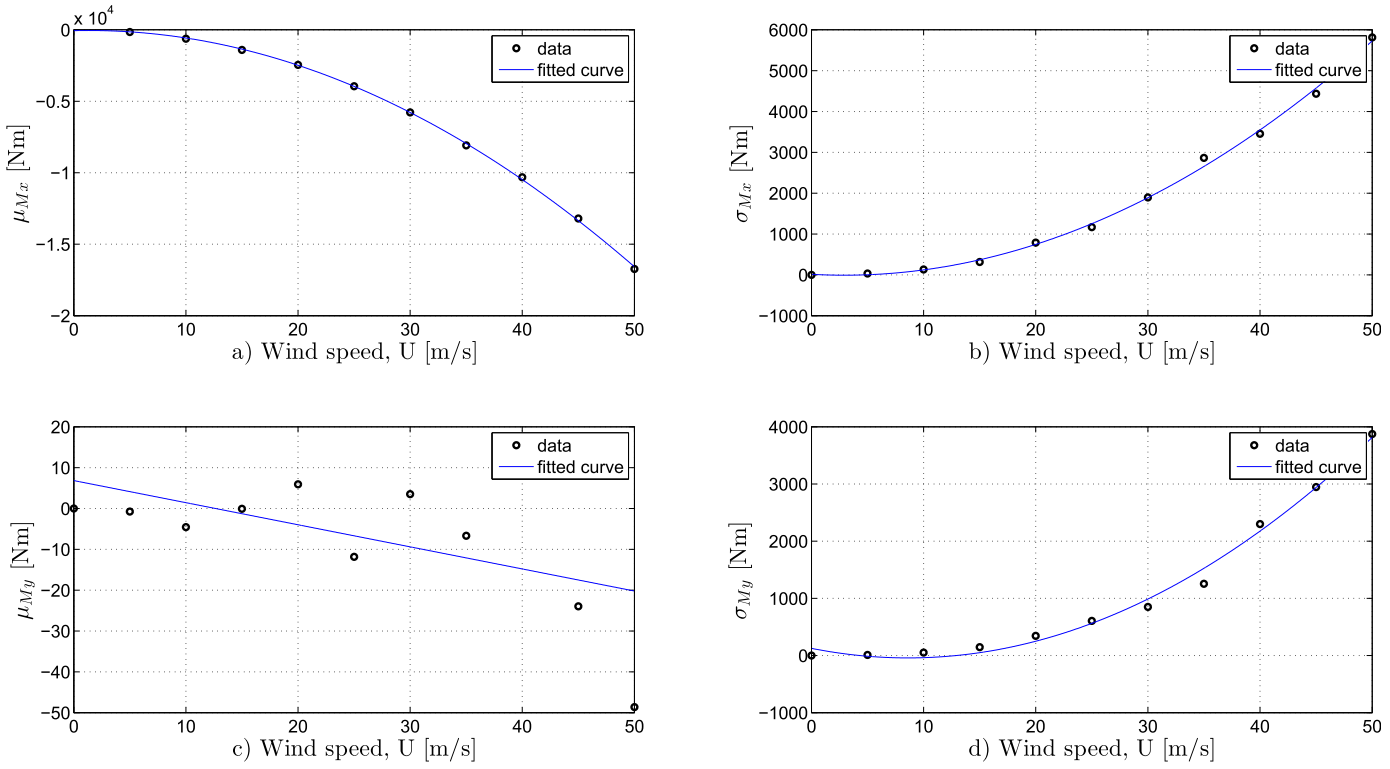

Fig. 4. Relation between mean nodal bending moments (μ_{M_x}, μ_{M_y}) vs. wind speeds (U) and standard deviation of nodal forces ($\sigma_{M_x}, \sigma_{M_y}$) vs. wind speeds ($U$) at 109.8 m of the tower under different wind speeds.

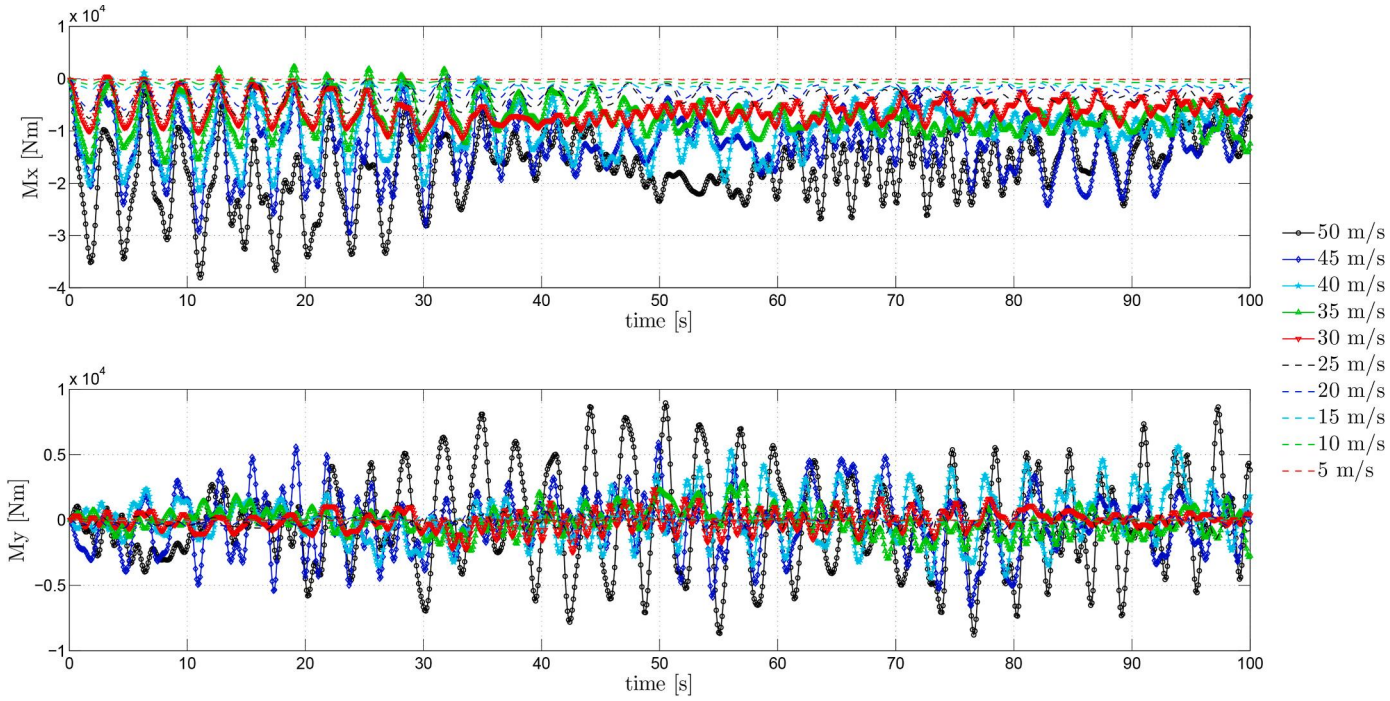

Fig. 5. Sample nodal force histories at 109.8 m of the tower under wind speeds varying from 5 to 50 m/s.

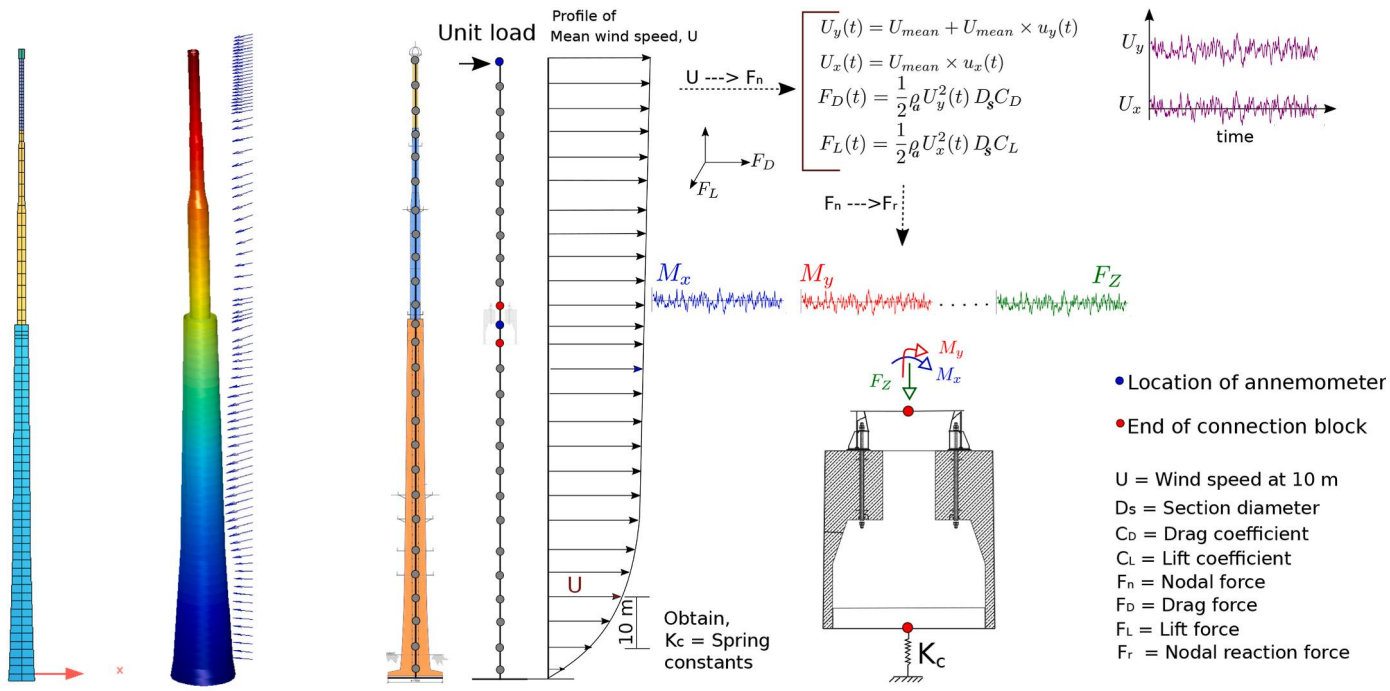

	Location of the nodes	Height of tower [m]
Top node of connection block (in steel)	2.3 m above reinforced concrete	109.8 (107.5+2.3 m)
Bottom node of connection block (in concrete)	4.195 m below reinforced concrete	103.305 (107.5-4.195 m)

Fig. 6. Methodology of coupling between the global model and local model.

loading generated from mean wind speed $U_{mean} = 15$ m/s is shown in Fig. 9. Because of the variable wind loading pattern, the simulation could not be reduced down to a symmetric analysis, making the numerical analysis extremely time and resource-consuming (the connection block model contains over 3 million degrees of freedom). To alleviate the computational inefficiencies, a response surface-based stress prediction is considered as an alternative, where at first, 1000 simulations with different time series were carried out using the global model to obtain nodal moments at various wind speeds. The outcome from these simulations is introduced as 'support point' in meta-modelling to establish a polynomial regression-based prediction model and is later used to retrieve the stress histories for any wind speed. Since the predicted stress is well below the yield limit, no material non-linearity is assumed in generating the polynomial model.

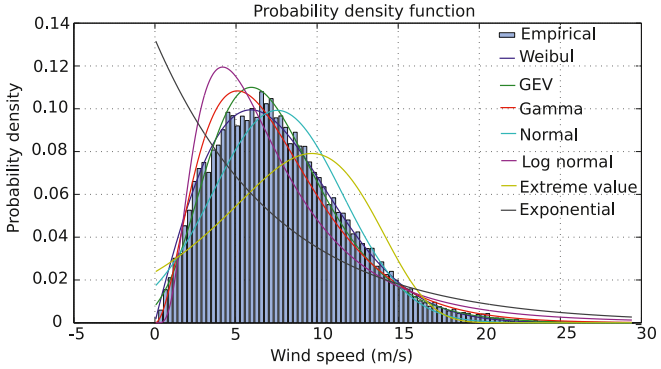

Distribution type	location	scale	shape	AIC	BIC
Weibull	-	8.51	1.96	162858.7	162875.3
Generalized extreme value	5.76	3.35	-0.05	163469	163493.8
Gamma	-	2.46	3.07	163616.3	163632.9
Normal	7.55	4.02	-	166462.5	166479.1
Lognormal	1.85	0.65	-	167936.3	167952.9
Extreme value	9.67	4.65	-	177364.8	177381.4
Exponential	7.55	-	-	178965	178973.3

Fig. 7. Right – Distribution type fitting to 205 days of mean 10-min wind speed data measured from the anemometer at +188 m; Left – Fitting different distribution type to the two years of wind data from the top anemometer.

Fig. 10 presents sample stress histories generated by a 10 min mean wind speed of 15 m/s among the bolts, where the left sub-figure shows the Von Mises stress, S_{vms} and the right figure shows the difference between mean stress and von Mises stress, $S_{vms} - S_m$. As expected, the four nodes of a single bolt do not produce the same stress due to wind load variation in different directions. From the right sub-figure, it is observed that the maximum variation concerning the mean stress occurs in node-3 of bolt-6 followed by node-4 of bolt-7, yet with maximum variation of 1 MPa. This small variation indicates that the fatigue damage to the bolts is not that significant. However, among the considered bolts, bolt-6 and bolt-7 are expected to have the maximum damage. Similarly, stress histories under other wind speeds can also be estimated, either directly from the numerical model or by implementing the fit equations established through polynomial regression, which will aid in fatigue life cycle assessment.

Since the von Mises stress, S_{vms}, is dependent on the nodal bending moments, M_x and M_y, the approximated model is expressed as $S_{vms} = p_0 + p_1 M_x + p_2 M_y$. In Table 4, the p_0, p_1, p_2 for all corresponding nodes of the bolts are listed. In Fig. 11, two fit surfaces for node-1 of bolt-6 and node-1 of bolt-15 have been plotted. The fit surfaces yield the goodness

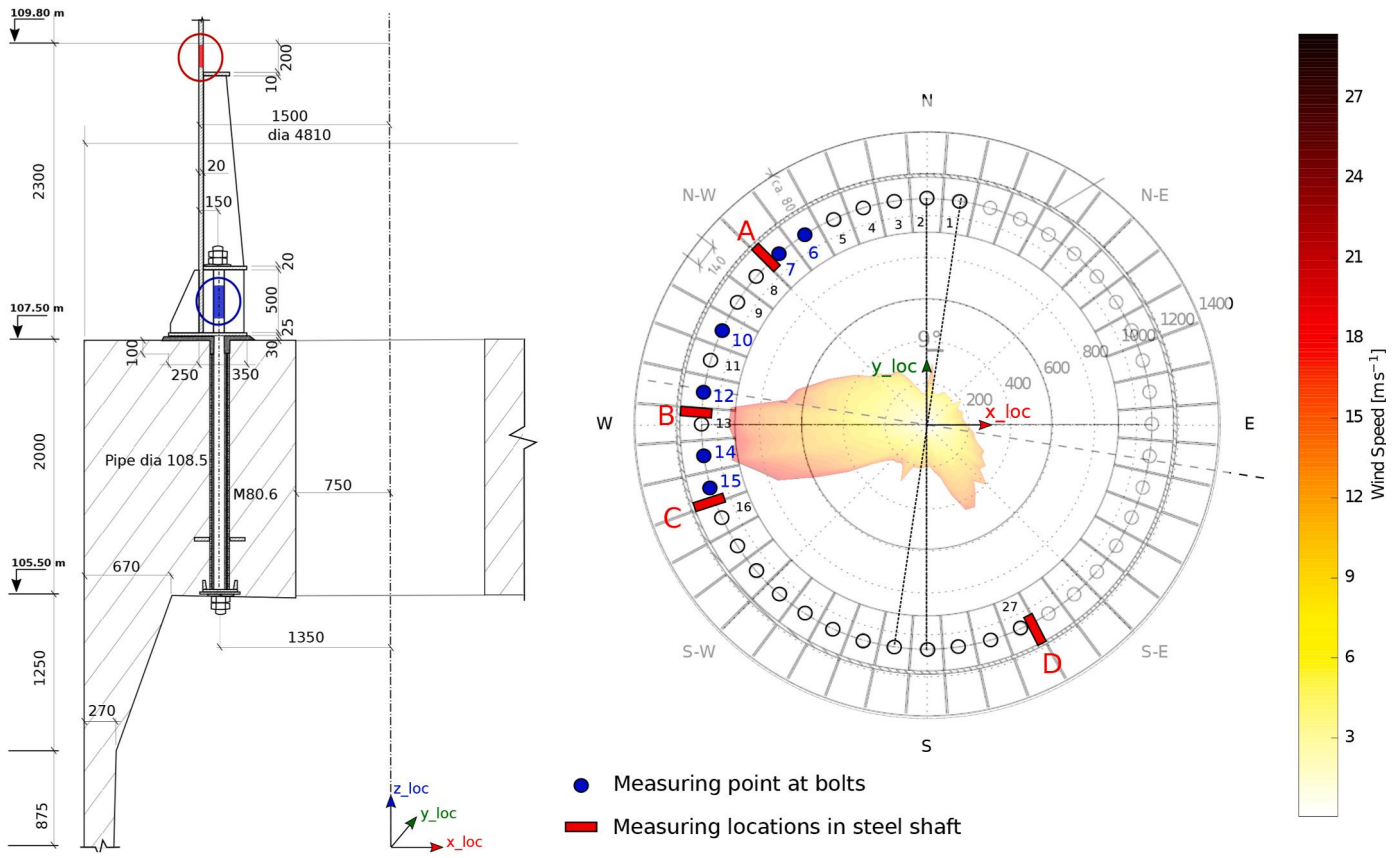

Fig. 8. The proposed locations for fatigue analysis - the blue colour represents the identified bolts and the red colour represents the identified locations on steel shaft. This study is limited to the damage analysis of the bolts. The section of the connection block is over-plotted on the polar wind speed direction to identify the best locations. (For interpretation of the references to colour in this figure legend, the reader is referred to the Web version of this article.)

of fit value, $\mathcal{R}^2 = 1$, because the input parameters are effectively two nodal moments (*Mx*, *My*) and the linear superposition of stress is adequate for service life analysis.

5. Stress-based fatigue analysis

The studied TV tower has been subjected to several inspection and monitoring programs since it came into service. In recent inspections, apart from concrete deterioration in the connection block, no noticeable cracks were found, neither in the steel-shaft, nor in the bolts. In this situation, the most appropriate fatigue design technique is the stress-life approach, which is defined as a high-cycle fatigue assessment given that the structural member can withstand more than 100,000 loading cycles within the material's elastic range.

5.1. Rainflow counting algorithm

The rainflow counting algorithm (RCA) is an essential tool, first proposed by Ref. [16], to convert a loading sequence of varying stress ratio into an equivalent set of constant amplitude stress reversals. Herein the mean stress, stress amplitudes, and frequency of different stress ranges can be obtained to estimate the fatigue life of a component. .

In RCA, the number of stress blocks used for analysis is generally user-specified, and based on this, the stress signals are broken down into distinct stress amplitudes and frequencies. As follows, the mean stress, stress amplitude, and the number of cycles is calculated using the frequency and amplitudes of different stress blocks by integrating them into RCA. This method is faster since the signal (in this case, the stress signal) is divided into numerous blocks, making the signal smaller, and the result is summed up at the end. The fundamental disadvantage of this traditional technique is that it does not account for the impacts of the loading sequence, which can result in the loss of some mean stress information, a crucial point in damage estimation. As a result, two RCA techniques are described here: one with breaking down the stress signal, termed as *without loading sequence*, and another without breaking down the loading signal, termed as *with loading sequence*. In this section, two separate days' wind histories are considered to illustrate, as shown in Fig. 12, on how integrating the loading sequence into the RCA can alter the rainflow matrix calculation.

A simple flowchart is shown in Fig. 14 to demonstrate how the loading sequence should be accounted for in RCA. Generally stating, in the conventional RCA, one variable amplitude (VA) signal is broken down into multiple constant amplitude (CA) signals with corresponding frequencies; the multiple CA signals are thereafter appended based on the stress amplitude and fed into the RCA to extract the rainflow matrix. A modified approach considered in this paper is that the CA signals are

Table 4
Orientation of the nodes in the bolts, geometrical locations, coefficients from the stress and nodal force relationship where the stress, $S_{vms} = p_0 + p_1.M_x + p_2.M_y$(Pa). The fit surfaces of the highlighted two nodes are shown in Fig. 11. The reference local coordinate system is indicated in Fig. 8.

Orientation of the bolt nodes w.r.t North(N) direction	Bolt no. (Figure 8)	Node no.	x_{loc} [m]	y_{loc} [m]	z_{loc} [m]	p_0	p_1	p_2
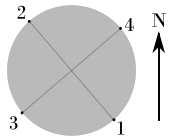	6	1 (1)	-0.851	0.996	4.514	29428072	0.235	0.269
		2 (2)	-0.903	1.057	4.514	32704130	0.464	0.446
		3 (3)	-0.906	0.999	4.514	31548733	0.336	0.809
		4 (4)	-0.845	1.051	4.514	30380437	0.35	-0.108
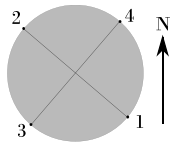	7	1 (5)	-0.996	0.851	4.509	30803152	0.282	0.756
		2 (6)	-1.057	0.903	4.509	32917780	0.398	0.406
		3 (7)	-1.051	0.845	4.509	32003025	0.04	0.325
		4 (8)	-0.999	0.906	4.509	31587742	0.633	0.328
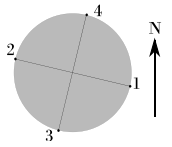	10	1 (9)	-1.274	0.306	4.514	29416014	0.031	0.357
		2 (10)	-1.352	0.324	4.514	32712417	0.114	0.633
		3 (11)	-1.32	0.276	4.514	31542084	-0.205	0.852
		4 (12)	-1.301	0.353	4.514	30382266	0.347	0.118
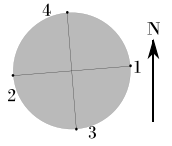	12	1 (13)	-1.306	-0.103	4.514	29412253	-0.08	0.348
		2 (14)	-1.386	-0.109	4.514	32712967	-0.088	0.639
		3 (15)	-1.34	-0.146	4.514	31541881	-0.459	0.748
		4 (16)	-1.347	-0.066	4.514	30378927	0.294	0.219
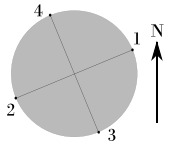	14	1 (17)	-1.21	-0.501	4.514	29424237	-0.183	0.306
		2 (18)	-1.284	-0.532	4.514	32704499	-0.282	0.58
		3 (19)	-1.23	-0.553	4.514	31548975	-0.666	0.57
		4 (20)	-1.26	-0.479	4.514	30376265	0.211	0.299
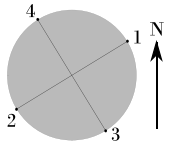	15	1 (21)	-1.117	-0.684	4.509	30803311	-0.156	0.348
		2 (22)	-1.185	-0.726	4.509	32917707	-0.264	0.504
		3 (23)	-1.128	-0.738	4.509	32002540	-0.297	0.138
		4 (24)	-1.17	-0.67	4.509	31587961	-0.117	0.703
* The node numbers in bracket are cumulative node number that will be used in Section 5.2								

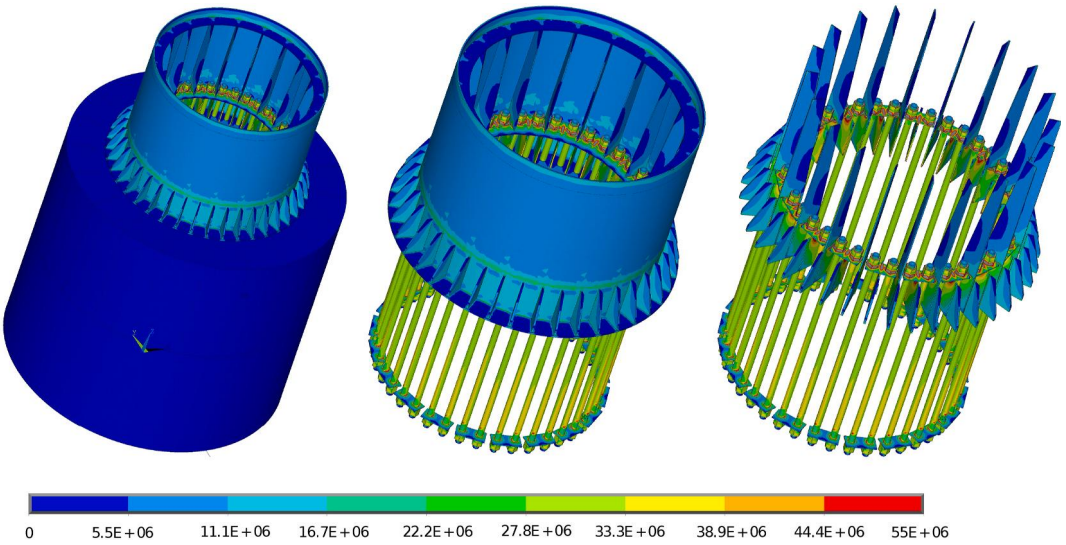

Fig. 9. A sample stress distribution in the connection block under loading generated from mean wind speed U_{mean} = 15 m/s.

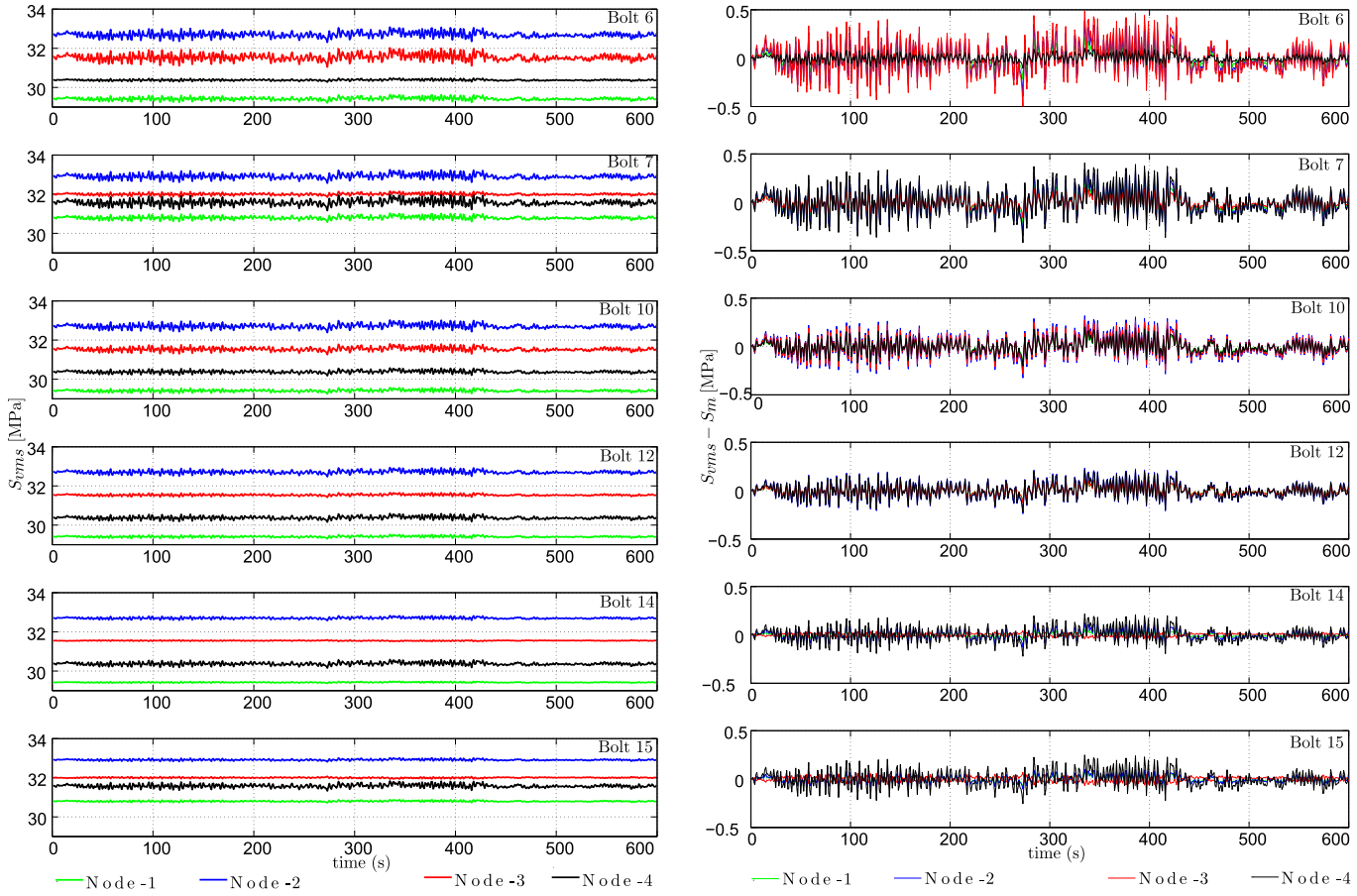

Fig. 10. Left: Von Mises stress S_{vms}, right: Resulted stress = (Von Mises stress, S_{vms} - mean stress, S_m) – obtained from the 3D volume-based finite element model at nodes of the selected bolts under 10 min mean wind speed, U_{mean} = 15 m/s.

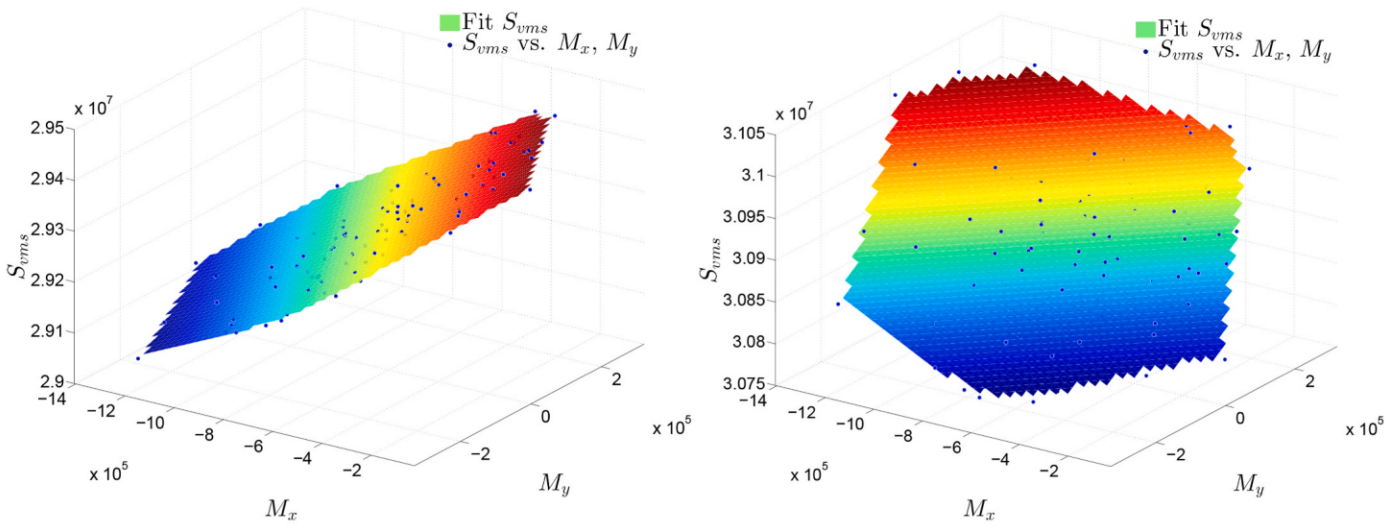

(a) Bolt number-6, node-1 (b) Bolt number-15, node number-1

Fig. 11. Polynomial regression based stress curves for node-1 of two different bolts. The parameters are listed and highlighted in Table 4.

not being appended based on the stress amplitude before introducing to RCA. Fig. 13 shows the stress history of node-15 (node-3 of bolt-12, see Table 4 for details) corresponding to wind loading depicted in Fig. 12 to demonstrate the difference between these two methodologies. In Fig. 13 (a) and (b), the red lines represent the signals used in RCA, and the blue lines represent the signals used in modified RCA. As it can be observed, by ignoring the loading sequence, some stress ranges are getting ignored, which usually are the big jumps in stresses due to abrupt changes in the wind flow.

The influence can be better observed in the produced rainflow matrices plotted in Fig. 15. Comparing the results from day-1, plotted in Fig. 15(a) and (b), it is clearly observed that, a few new entries appear in the rainflow matrix considering loading sequence, which correspond to additionally identified stress ranges and mean stress. A similar trend is also observed for day-2 by comparing the results plotted in Fig. 15(c) and (d)-here, the stress range $\Delta S_R \geq 15$ MPa shows some additional entries. The inclusion of these new stress ranges will evidently increase the damage accumulation for life cycle assessment and will be discussed in the next section.

5.2. Fatigue damage accumulation

The Palmgren–Miner linear damage hypothesis, often known as Miner's rule, was proposed by Palmgren in 1924 [19] but popularised by Miner in 1945 [20], is widely used to estimate the fatigue damage calculation. According to this rule, a linear damage accumulation law subjected to a variable stress history is defined by the following formula

$$D_d = \sum_i^k \frac{n_i}{N_i} \tag{6}$$

where n_i is the number of cycles at a stress level S_i, N_i is the number of cycles required for failure at a stress level S_i, and k is the number of stress levels identified in a stress time history at the corresponding structural point. The number of cycles N_i required for failure regarding the stress level S_i is described using the S–N fatigue curves, which are derived from laboratory experiments on simple specimens subjected to constant amplitude loads. The number of cycles N_i at a given stress level S_i is commonly calculated by applying RCA, discussed in section 5.1, to the stress time histories recorded or approximated for the point under consideration.

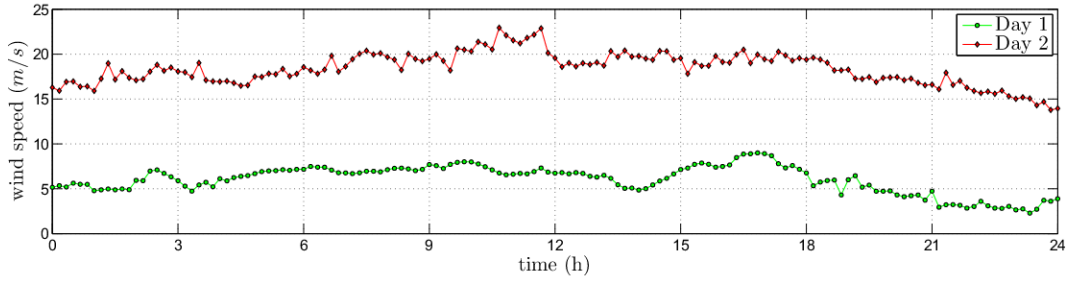

Fig. 12. Wind speed of two independent days monitored at 188 m of the tower.

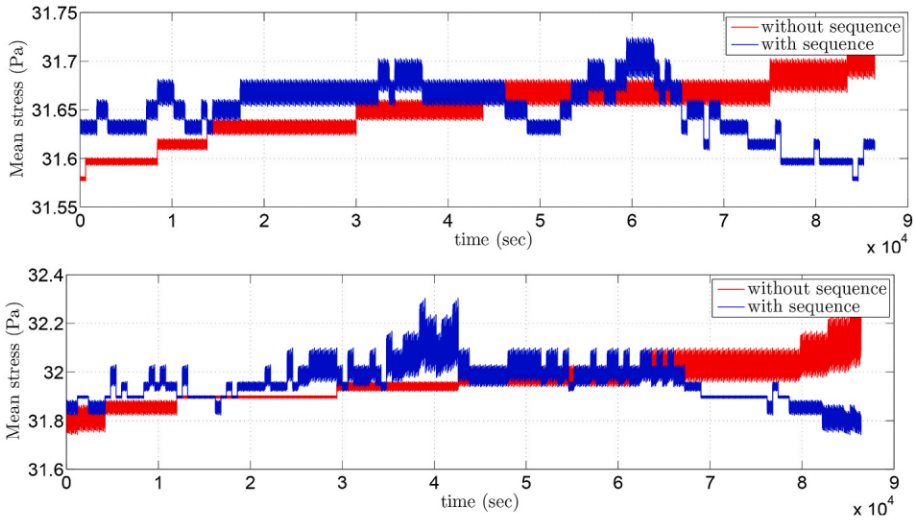

Fig. 13. Mean stress information for rainflow counting algorithm at node-15 (node-3 of bolt-12, see Table 4) at Day-1 (top) and at Day-2 (bottom), with and without loading sequence.

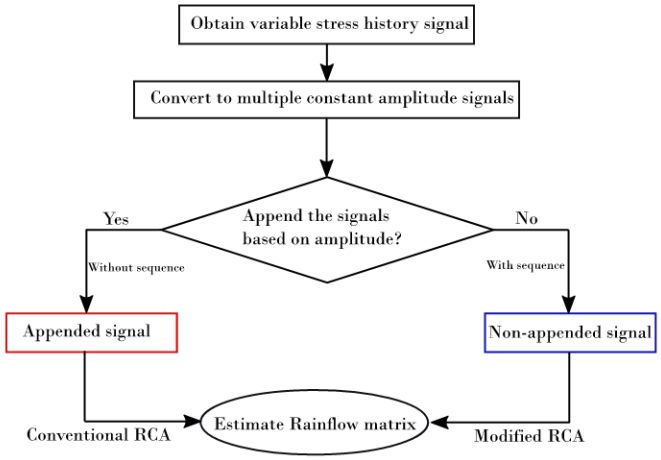

Fig. 14. Flowchart to represent the loading sequence effects on RCA analyses.

The fatigue damage of a structural detail is determined by the stress range spectrum (stress range S and number of stress cycles n), according to Miner's rule. In Eurocode 3 [38], the fatigue detail category is classified as follows:

$$D_d = \sum_{j=1}^{k_1} \frac{n_i}{5 \times 10^6} \left(\frac{\Delta S_i}{\Delta S_D}\right)^m + \sum_{j=1}^{k_2} \frac{n_j}{5 \times 10^6} \left(\frac{\Delta S_j}{\Delta S_L}\right)^{m+2} \tag{7}$$

where ΔS_D is the constant amplitude fatigue limit at 5×10^6 cycles; ΔS_L is the cut-off limit; ΔS_i and ΔS_j are the ith and the jth stress ranges, n_i and n_j are the number of cycles in each ΔS_i and ΔS_j block, m is the slope of the curve, and k_1 and k_2 represent the number of different stress range blocks above or below the constant amplitude fatigue limit ΔS_D.

Each fatigue detail category addressed in Eurocode 3 is assigned a number that provides the reference value ΔS_C for fatigue strength at 2 million loading cycles in N/mm^2. The fatigue detail category 50 is used to show the method because this study focuses on the accuracy of the fatigue damage predicted by the suggested method. Eurocode 3 recommends the following values for the parameters of the design S–N curves for bolted constructional detail category - 50: $m = 3$, $\Delta S_D = 41.63$ MPa, and $\Delta S_L = 37.89$ MPa. The specifics of the fatigue strength curves for direct stress ranges are shown in Fig. 16(a), with the details category - 50 for bolted constructional detail highlighted in red. However, the detail category must be corrected based on the bolt diameter and surface adjustment.

Since the bolts are of M80.6 mm, the following correction has been applied for increased diameter:

$$\Phi = \text{bolt diameter} = 80mm$$

$$\text{Size effects for } \Phi > 30\ mm,\ k_s = \left(\frac{30}{\Phi}\right)^{0.25} = \left(\frac{30}{80}\right)^{0.25} = 0.78254$$

$$\Delta S_{C,red} = k_s \times \Delta S_C = 0.7825 \times 50 = 39 \text{ MPa}$$

Because fatigue fractures normally begin at the surface, the surface quality has a significant influence on the component's life. On a rougher surface, a fatigue crack gets initiated faster than on a smoother surface. Therefore, surface correction is taken into account in addition to bolt diameter correction, as illustrated in Fig. 16(b). The surface correction factor, k_f, is chosen as 0.9 for fine ground or commercially polished surfaces, resulting in the stress range:

$$\Delta S_{C,red,2} = k_f \times \Delta S_C = 0.9 \times 39 = 35 \text{ MPa}$$

Therefore, for the damage accumulation calculation, the corrected detail category - 35 is used with $m = 3$, $\Delta S_D = 29.14$ MPa and $\Delta S_L = 16$ MPa.

As stated in section 5.1, the damage accumulation is estimated independently for two days with distinctive wind profiles and is shown in Fig. 17. Damage for Day-1 is indicated in Fig. 17(a) with the highest damage observed in node-3 (bolt-6), and for Day-2 in Fig. 17(b) with the highest damage in node-8 (bolt-7). In general, nodes 1–12 (bolts 6, 7, 10) show higher damage compared to nodes 13–24 (bolts 12, 14, 15). Despite the similar stress amplitudes among the bolts, bolts 6, 7, and 10 face higher damage due to their larger stress range, the most important

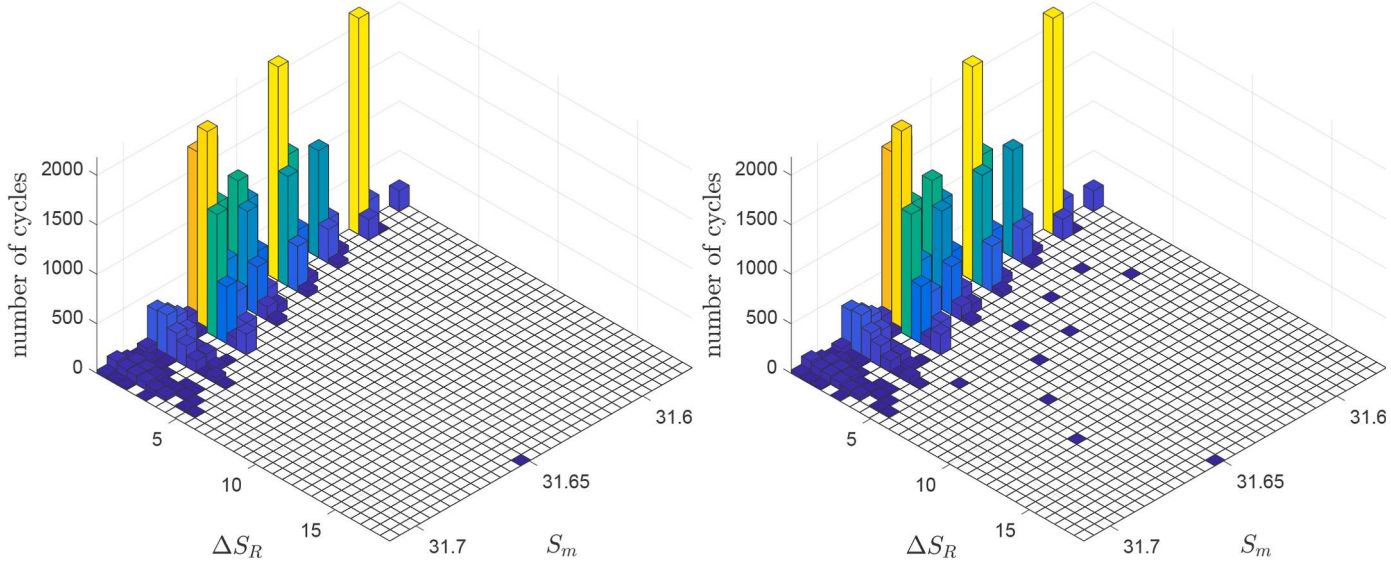

(a) Day 1 - without loading sequence

(b) Day 1 - with loading sequence

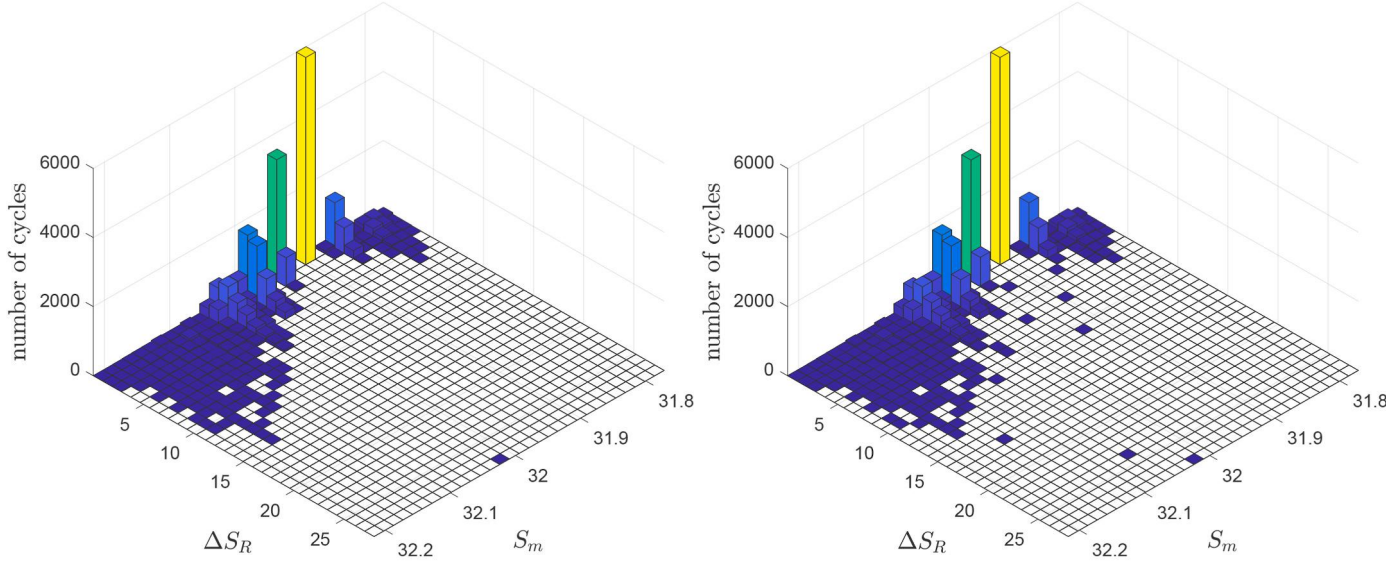

(c) Day 2 - without loading sequence

(d) Day 2 - with loading sequence

Fig. 15. Rainflow matrices containing the mean stress S_m, stress amplitude ΔS_R and number of loading cycle, of two single days (node-3 of bolt-12) showing the impact of loading sequence on the rainflow calculation.

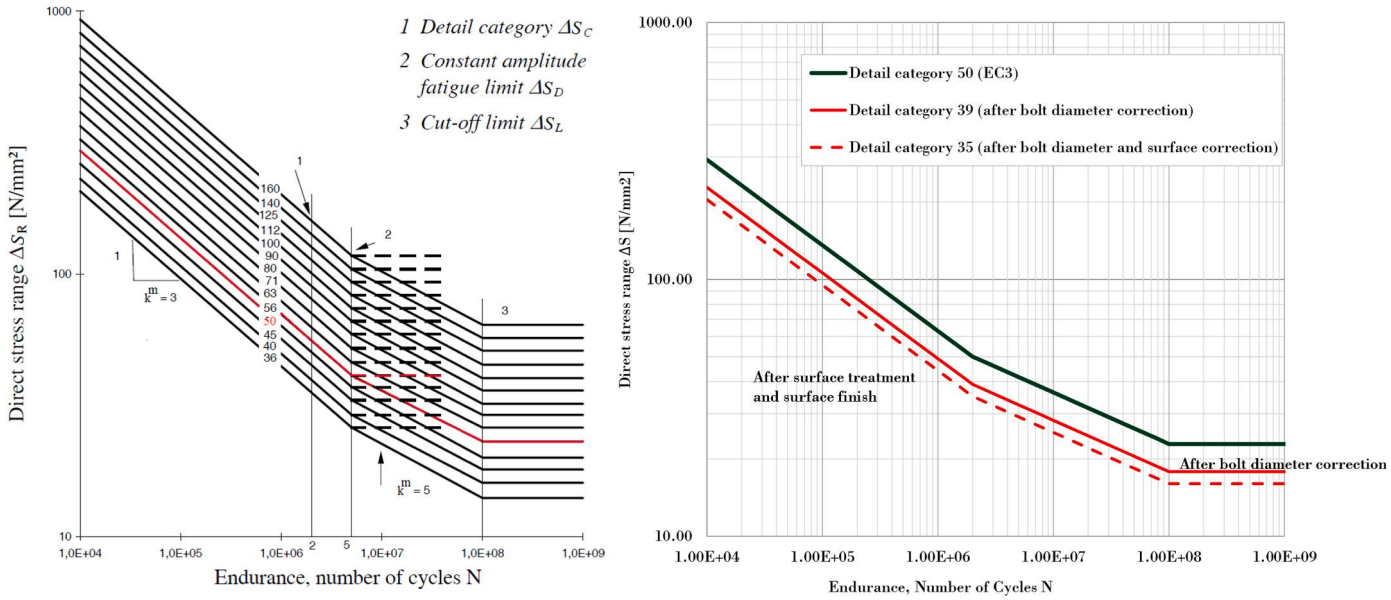

(a) Fatigue strength curves for direct stress ranges (b) After correction for bolt diameter and surface finish

Fig. 16. The corrected details category - 35 for bolted constructional detail as per Eurocode 3 [38].

parameter for creating the differences. On the contrary, bolts away from this position, in this case, bolts 12, 14, and 15, have lower stress ranges and thus the accumulated damage.

At first glance, there isn't much of a difference between the predicted damage with RCA and modified RCA. Therefore, the percentage of difference is plotted additionally. Given that the mean stress in these nodes varies between 31.5 and 32.5 MPa, i.e., the stress ratio R is close to 1, the highest variation in damage of roughly 4% is seen in node-15 (bolt-12) for Day-1 and node-17 (bolt-14) for Day-2. In terms of fatigue, $R = 1$ denotes a structural component with a nearly constant stress state and minimal fatigue damage. Despite this, the proposed modification in RCA generates a maximum 4% of difference in damage calculations, which implies that the signals with higher stress variations (where $R = 0$ to -1) would produce larger differences. Presumably, the effect on overall damage would be substantially significant if measured over 50 years instead of 1 day.

The damage for 50 years is estimated considering different approaches and represented in Fig. 18. The tower has been monitored for one year, however only 205 days of data are used in this calculation. The minimum and maximum 10-min mean wind speeds during this period recorded were 0.05 and 29.41 m/s, respectively, with Weibull as the best-fit distribution, as shown in Fig. 7. Based on this information, a stochastic distribution of 50 years of wind speed is generated for this tower. The damage is initially determined with conventional RCA and is termed as *damage no sequence* in Fig. 18. To account for loading sequence effects, the variation between the RCA and modified RCA is estimated for 205 days, and the same variation is introduced in 50 years of analysis, hence termed as max *possible damage with sequence (based on 205 days of data)* and min *possible damage with sequence (based on 205 days data)*. It is important here to mention that, without a monitoring scheme, it would not be possible to estimate the variation that occurs due to considering the loading sequence effect. However, the variation observed in 205 days of monitored data may not be representative of the variation seen over 50 years and is not possible to predict. As a result, a conservative approach is taken, in which the variation of 205 days is multiplied by 2, essentially widening the range of probable damage accumulation. The newly defined damages are termed as max *possible damage with sequence* and min *possible damage with sequence*.

The maximum damage among the four nodes indicates the decisive damage state of a single bolt. For example, nodes 1–4 correspond to bolt-6 and the maximum damage is observed in node-3, with a maximum of 6.6×10^{-4} with conventional RCA, and a maximum of 7.75×10^{-4} with modified RCA(max *possible damage with sequence based on 205 days of data*), shown in Fig. 18. In general, it is observed that the stresses in bolts are extremely low and the total damage of 50 years suggests that the bolts have no risk of damage due to fatigue. The differences in total damage accumulation between conventional RCA (*damage no sequence*) and modified RCA (max *possible damage with sequence based on 205 days of data*), are plotted in Fig. 19. A notable difference is observed between the two methods, with approximately 20% more damage with the modified method for bolts 6, 7, and 8—which are set in the along-wind direction and face relatively more damage. On the contrary, in bolts 12,14, and 15—which are located in the cross-wind direction, the damage is comparatively lower, yet the impact of the loading sequence is much more significant. The damage is more than twice as much in node-15 of bolt-12 owing to the loading sequence effect. Modification applied to the conventional RCA, therefore, can capture the damage scenarios that are otherwise being ignored and, as such, represent the remaining capacity of the structure more appropriately.

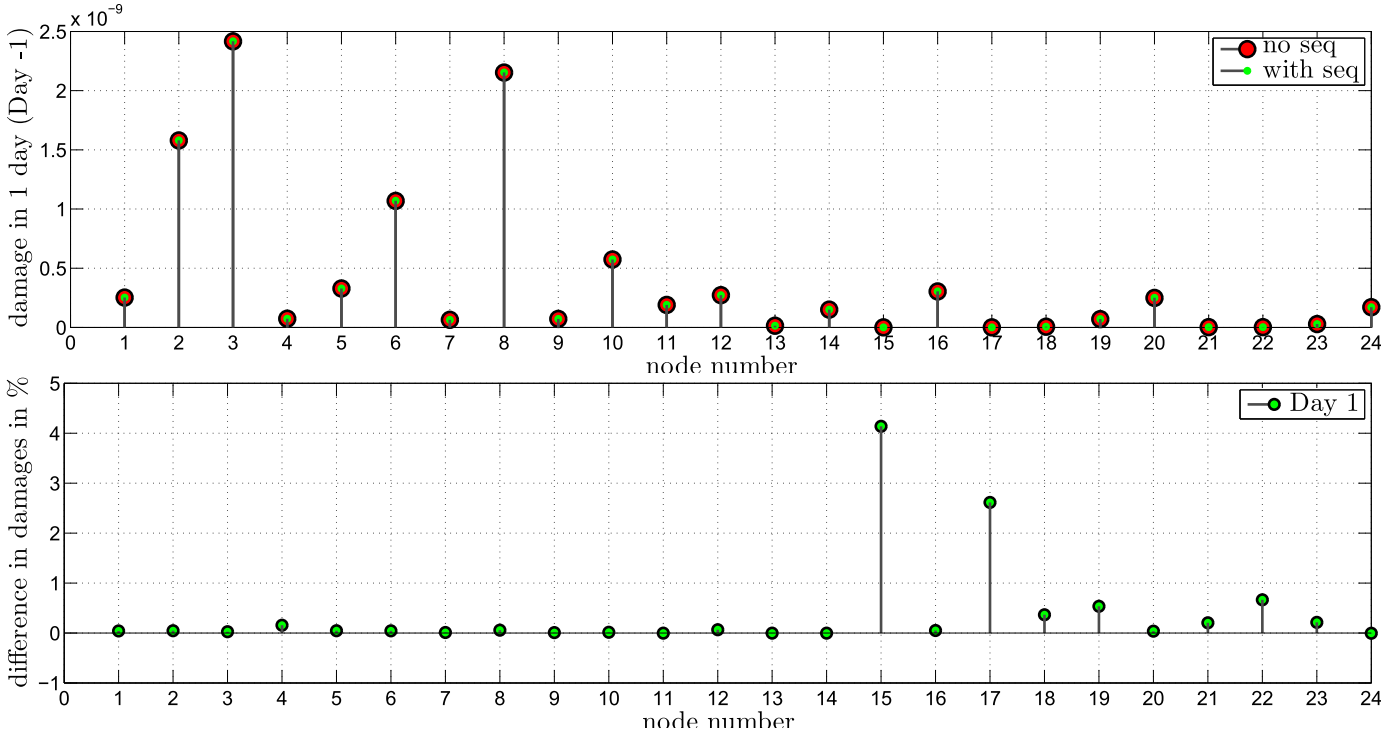

(a) The top figure shows the damage in Day-1 without and with considering loading sequence whereas the bottom figure shows the % of differences in damage accumulation between the two methods

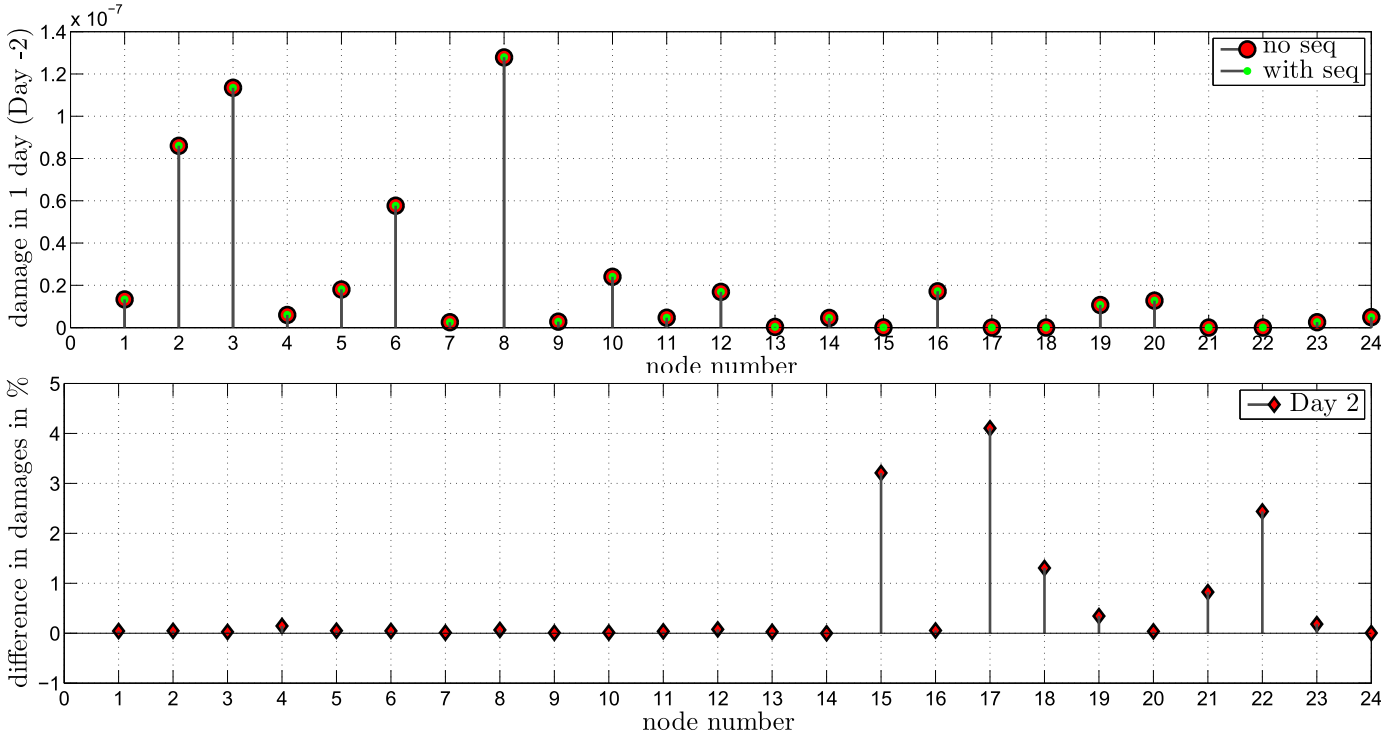

(b) The top figure shows the damage in Day-2 without and with considering loading sequence whereas the bottom figure shows the % of differences in damage accumulation between the two methods

Fig. 17. Damage accumulation based on Palmgren-Miner's rule for two individual days.

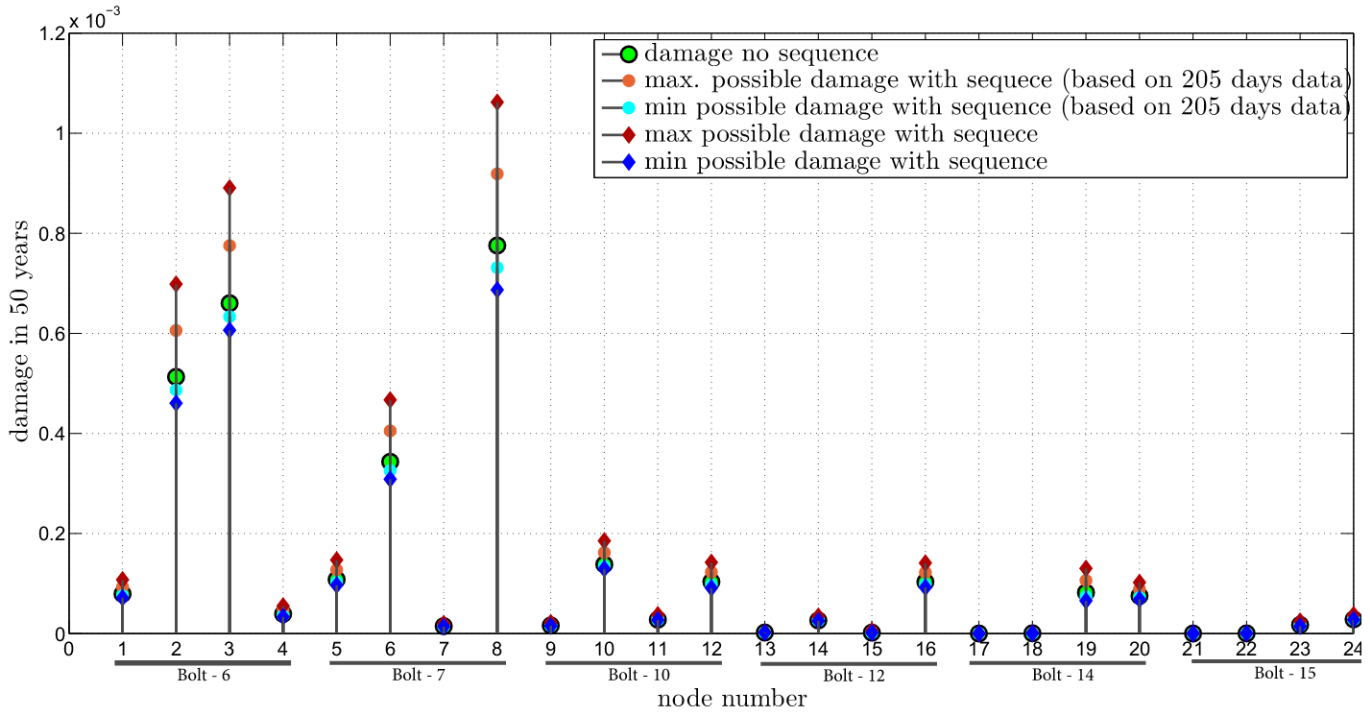

Fig. 18. Total damage accumulation for 50 years - with conventional RCA *(damage no sequence)*, and with modified RCA *(considering loading sequence, where variation is based on 205 days monitoring data, and later variation is based on 50 years of artificially generated data)*.

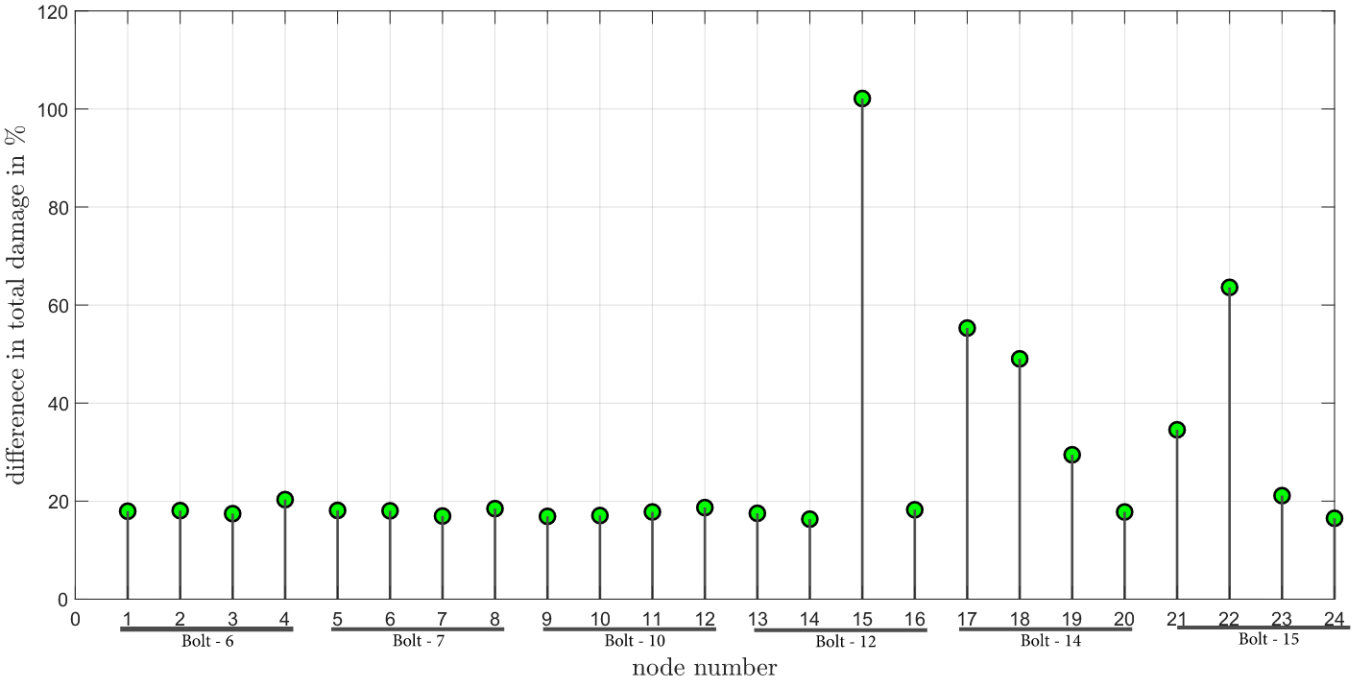

Fig. 19. Difference in total damage accumulation between conventional RCA (*damage no sequence*) and modified RCA (max *possible damage with sequence based on 205 days of data*).

6. Conclusions

This paper presents a practical approach to fatigue life cycle assessment of a bolted connection between reinforced concrete and steel section in 193 m tall TV tower subjected to wind loading, primarily emphasizing the bolts as per the authority's interest. For fatigue assessment, the rainflow counting algorithm (RCA) is applied, to which a modification is proposed for incorporating the loading sequence effects and has proven to be of significant importance in the damage accumulation.

The TV tower was under monitoring with anemometers and accelerometers installed, from which the retrieved wind data over a period of 205 days was used to establish that the best stochastic wind distribution is Weibull, and the decisive wind phenomena based on the *root mean square acceleration to wind speed relation* is Buffeting action. Based on the wind-rose diagram, 6 bolts are chosen — 3 of them in the along-wind direction and 3 of them in the across-wind direction, on which further investigations are carried out. The stresses from the selected bolts are deduced from numerical simulation by coupling a global tower model with a local yet very detailed connection block model consists of three million degrees of freedom. For deriving stress under a variable amplitude wind loading profile, advanced numerical analysis combined with meta-modelling technique was proven to be practical and computationally productive.

Bolts placed in the along-wind direction receive higher von Mises stresses with lower ranges, which shows that the damage accumulation for these bolts are approximately 6 times lower compared to the bolts in the cross-wind direction. The widely adopted RCA is integrated for damage calculation based on the Palmgren-Miner rule. Among the studied bolts, the maximum damage for 50 years is observed in one of the bolt placed in cross-wind direction of 1×10^{-3}, which is substantially below the level of concern. This paper has presented a modification to the conventional RCA to integrate the loading sequence effect, and within the scope of this study, it is shown that the estimated damage is increased on an average by 20% for the along-wind direction bolts and up to 100% for the cross-wind direction bolts. Incorporating loading sequence in the conventional RCA is therefore proven to be a safer alternative in terms of fatigue assessment.

Based on the outcome of this study, further investigations would be focused on developing benchmark cases where the difference between conventional and modified RCA would be investigated by varying several parameters in random stress signals. Also, considering the life cycle assessment of the monitored structure, additional studies would be conducted on including further parameters, such as uncertainty from the measurement data, such that a more reliable and precise damage estimation can be obtained.

Credit author statement

S. Chowdhury: Conceptualization, Methodology, Software, Validation, Formal analysis, Investigation, Resources, Data curation, Writing – original draft, Writing – review & editing, Visualization. V. Zabel: Validation, Resources, Writing – review & editing, Supervision, Project administration, Funding acquisition.

Declaration of competing interest

The authors declare that they have no known competing financial interests or personal relationships that could have appeared to influence the work reported in this paper.

Acknowledgments

The authors gratefully acknowledge the contribution from Dr.-Ing. Tajammal Abbas on the buffeting analysis of the tower. Financial support for this work was provided by the German Research Foundation (DFG), within the research training group 1462. This support is gratefully acknowledged. This article was funded by the Open-Access Publishing Programme of the German Research Foundation (DFG) and the publication fund of the Bauhaus-Universität Weimar.

References

[1] M. Repetto, G. Solari, et al., Crosswind Response Induced Fatigue of Slender Structures, 2000.
[2] M.P. Repetto, G. Solari, Dynamic crosswind fatigue of slender vertical structures, Wind Struct. 5 (6) (2002) 527–542.
[3] A. Davenport, The estimation of load repetitions on structures with application to wind induced fatigue and overload, in: RILEM International Symposium on the Effects of Repeated Loading of Materials and Structures, Sep, 1966, pp. 1–18.
[4] M. Dionne, A. Davenport, A simple relationship between the gust response factor and fatigue damage, J. Wind Eng. Ind. Aerod. 30 (1–3) (1988) 45–54.
[5] S.H. Crandall, W.D. Mark, Random Vibration in Mechanical Systems, Academic Press, 2014.
[6] A.A. Petrov, Dynamic response and life prediction of steel structures under wind loading, J. Wind Eng. Ind. Aerod. 74 (1998) 1057–1065.
[7] M. Mikitarenko, A. Perelmuter, Safe fatigue life of steel towers under the action of wind vibrations, J. Wind Eng. Ind. Aerod. 74 (1998) 1091–1100.
[8] O. Flamand, J. Bietry, C. Barre, E. Germain, P. Bourcier, Fatigue calculation on the roof sustaining cables of a large stadium in paris, J. Wind Eng. Ind. Aerod. 64 (2–3) (1996) 127–134.
[9] P. Van Staalduinen, Wind loading and fatigue of steel framed masts, in: Moan, et al. (Eds.), Structural Dynamics, EURODYN, vol. 93, 1993, pp. 1107–1113.
[10] K.S. Kumar, T. Stathopoulos, Fatigue analysis of roof cladding under simulated wind loading, J. Wind Eng. Ind. Aerod. 77 (1998) 171–183.
[11] M. Gu, Y.L. Xu, L. Chen, H. Xiang, Fatigue life estimation of steel girder of yangpu cable-stayed bridge due to buffeting, J. Wind Eng. Ind. Aerod. 80 (3) (1999) 383–400.
[12] M.P. Repetto, G. Solari, Dynamic along wind fatigue of slender vertical structures, Eng. Struct. 23 (12) (2001) 1622–1633.
[13] M. Mahendran, Towards an appropriate fatigue loading sequence for roof claddings in cyclone prone areas, Eng. Struct. 17 (7) (1995) 476–484.
[14] P. Mendes, J.A. Correia, A.M. De Jesus, B. Ávila, H. Carvalho, F. Berto, A brief review of fatigue design criteria on offshore wind turbine support structures, Frat. Ed. Integrità Strutt. 15 (55) (2021) 302–315.
[15] C. Yuan, J. Li, Y. Xie, W. Bai, J. Wang, Investigation on the effect of the baseline control system on dynamic and fatigue characteristics of modern wind turbines, Appl. Sci. 12 (6) (2022) 2968.
[16] M. Matsuishi, T. Endo, Fatigue of metals subjected to varying stress, Jpn. Soc. Mech. Eng. Fukuoka, Japan 68 (2) (1968) 37–40.
[17] A. Niesłony, Determination of fragments of multiaxial service loading strongly influencing the fatigue of machine components, Mech. Syst. Signal Process. 23 (8) (2009) 2712–2721.
[18] A. Nieslony, Rainflow Counting Method, Set of Functions with User Guide for Use with MATLAB, 2010. Information on http://www. mathworks.com/matlabcentral/fileexchange/3026.
[19] A. Palmgren, Die Lebensdauer von Kugellagern. z. VDI 68, vol. 68, VDI-Zeitschrift, Veifahrenstechinik, Berlin, 1924, pp. 339–341.
[20] M. Miner, Cumulative damage in fatigue, J. Appl. Mech. 3 (1945) 159–164.
[21] G. Bolzon, V. Buljak, An effective computational tool for parametric studies and identification problems in materials mechanics, Comput. Mech. 48 (6) (2011) 675–687.
[22] A.A. Mullur, A. Messac, Metamodeling using extended radial basis functions: a comparative approach, Eng. Comput. 21 (3) (2006) 203.
[23] A. Kareem, S. Kabat, F.L. Haan Jr., Aerodynamics of nanjing tower:: a case study, J. Wind Eng. Ind. Aerod. 77 (1998) 725–739.
[24] V. Popov, J. Valivonis, A. Šapalas, G. Šaučiuvėnas, T. Urbanavičius, T. Šlivinskas, Application of numerical methods for the analysis of a concrete-steel tower subjected to multiple load factors, Procedia Eng. 57 (2013) 914–921.
[25] H. Kawai, Vortex induced vibration of tall buildings, J. Wind Eng. Ind. Aerod. 41 (1–3) (1992) 117–128.
[26] H. Marukawa, N. Kato, K. Fujii, Y. Tamura, Experimental evaluation of aerodynamic damping of tall buildings, J. Wind Eng. Ind. Aerod. 59 (2–3) (1996) 177–190.
[27] S. Pospíšíl, J. Lahodnỳ, V. Janata, S. Urushadze, R. Král, S. Hračov, Lifetime Prediction of Wind Loaded Mast and Towers with Respect to Lateral and Longitudinal Wind Spectrum, Engineering Mechanics, 2012, p. 96.

[28] G. Piccardo, 3-d gust effects on slender vertical structures, Proc. 4th Int. Coll. Bluff Body Aerodynam. Appl. (2000) 285–288.
[29] E.S. Association, et al., Guidelines for safe seal usage-flanges and gaskets, Report No, ESA/FSA 9 (98) (1998) 1–40.
[30] ANSYS Users Manual, ANSYS Mechanical APDL Technology Demonstration Guide, Canonsburg, ANSYS Inc, USA, 2013.
[31] ANSYS Mechanical APDL Contact Technology Guide, Online Documentation, 2013.
[32] T. Abbas, Assessment of Numerical Prediction Methods for Aeroelastic Instabilities of Bridges, PhD. Thesis, Bauhaus University, Weimar, 2016.
[33] S. Marwitz, V. Zabel, Relations between the Quality of Identified Modal Parameters and Measured Data Obtained by Structural Monitoring, ISMA International Conference on Noise and Vibration Engineering, Leuven, Belgium, 2018.
[34] E. Simiu, R.H. Scanlan, Wind Effects on Structures, Wiley, 1978.
[35] Y.-L. Xu, Wind Effects on Cable-supported Bridges, John Wiley & Sons, 2013.
[36] T. Von Karman, Progress in the statistical theory of turbulence, Proc. Natl. Acad. Sci. U. S. A 34 (11) (1948) 530.
[37] B. Standard, Eurocode 1: Actions on Structures, 2005.
[38] B. Standerd, Eurocode 3: Design of Steel Structures-Part 1-9, 1993, pp. 1–9. Fatigue, BS EN.